PAPER • OPEN ACCESS

Symmetry-dependent carrier relaxation dynamics and charge–density–wave transition in DyTe$_3$ probed by polarized femtosecond spectroscopy

View the article online for updates and enhancements.

Symmetry-dependent carrier relaxation dynamics and charge–density–wave transition in DyTe$_3$ probed by polarized femtosecond spectroscopy

S Tsuchiya[1], Y Sugawara[1], S Tanda[1,2] and Y Toda[1]

[1] Department of Applied Physics, Hokkaido University, Sapporo, Hokkaido 060-8628, Japan
[2] Center of Education and Research for Topological Science and Technology, Hokkaido University, Sapporo 060-8628, Japan

E-mail: satoshi.tsuchiya@eng.hokudai.ac.jp

Abstract

Photo-induced quasi-particle (QP) relaxation dynamics with different symmetries have been investigated for the multiple charge–density–wave (CDW) compound DyTe$_3$ by using ultrafast polarized pump-probe spectroscopy. By performing symmetry analysis, the QP dynamics with isotropic A$_{1g}$ and anisotropic B$_{2g}$ symmetry were found to show unique anomalies at the first and second CDW transitions. Both the temperature dependence and pump fluence dependence indicate that the B$_{2g}$ response is very sensitive to the underlying lattice deformation, which provides critical insight into the multiple CDW formations.

Keywords: time resolved reflection spectroscopy, charge–density–wave systems, optical properties

1. Introduction

Optical pump-probe time-resolved spectroscopy has been widely used to study chemical reaction, [1] dynamics of photo-excitation in semiconductors [2, 3] and optical devices [4, 5], and photo-induced phase transition in spin-crossover solid [6, 7] and strongly correlated electron systems [8, 9]. Moreover, the pump-probe spectroscopy has made a great contribution to researches of the coexistence and competition of different kinds of ordered states such as superconductivity (SC) and pseudogap (PG) state in cuprate superconductors [10, 11]. When multiple ordered states co-exist together, those photo-excited quasi-particle (QP) dynamics can be distinguished from each other by differences in relaxation time, magnitude of transmission/reflectivity changes, and the temperature dependences between them [12–17, 19–29].

Recently, the coexistence of multiple charge–density–waves (CDW) has been reported in quasi-two-dimensional (Q2D) rare-Earth tritelluride compounds, RTe$_3$, where R is a rare-Earth ion (R = Dy, Ho, Er, Tm). RTe$_3$ consists of square planar Te sheets (a–c plane) and insulating RTe$_3$ layers, which are alternately stacked along the b direction [30]. The weakly interacting 5p electrons of the Te atoms construct a Q2D Fermi surface. Electron and x-ray diffraction measurements and angle-resolved photoemission spectroscopy (ARPES) have revealed that, in these compounds, the first CDW occurs along the c axis at high temperatures and the second CDW forms along the direction perpendicular to the first CDW direction (the a axis) at low temperatures [31–33]. However, in the pump-probe measurements for the series of RTe$_3$, the temperature dependence of the magnitude of transient reflectivity changes and relaxation time did not show clear evidence of the second CDW transition [34]. This is because the response associated with the second CDW formation can be buried in that of the first one. Thus, the QP dynamics of multiple CDW states have not been completely understood so far.
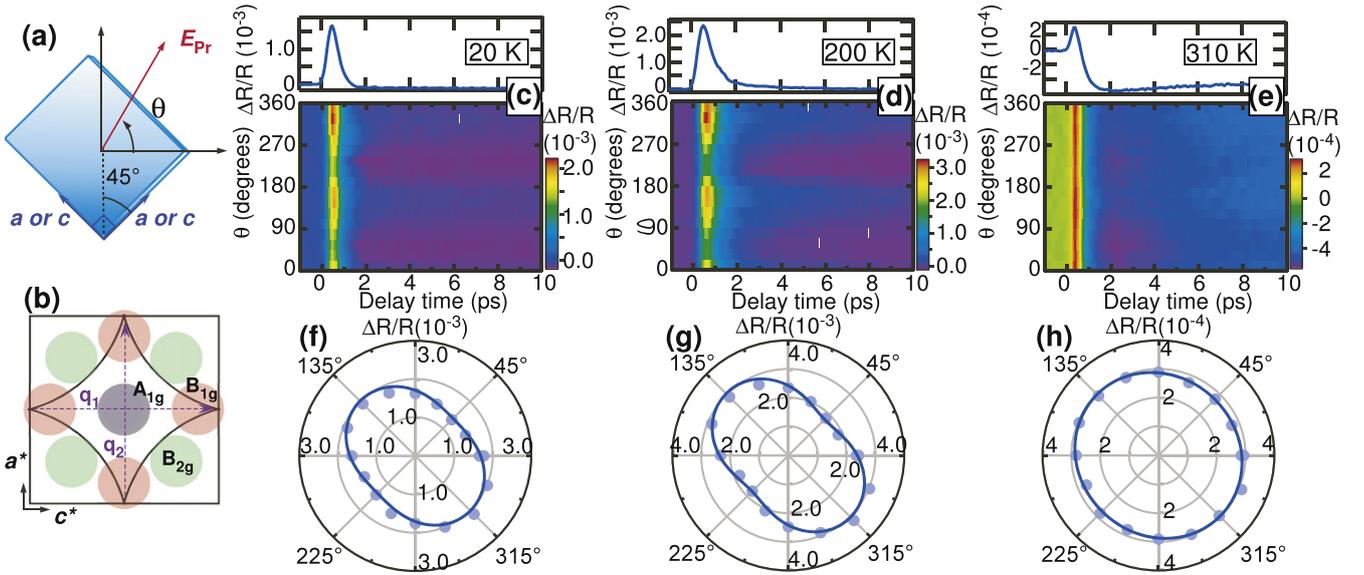
Figure 1. (a) Schematic of definition of the probe polarization angle θ. (b) Schematic of the Fermi surface and nesting vectors $\boldsymbol{q}_1$ and $\boldsymbol{q}_2$. A_{1g}, B_{1g}, and B_{2g} indicate the selectivity of the probe in the k-space according to the Raman-like process. (c)–(e) Intensity plots of $\Delta R/R$ transient for $F = 36\,\mu\text{J cm}^{-2}$ as a function of angle at 310, 200, and 20 K, respectively. (f)–(h) Polar plots of the maximum values of $\Delta R/R$.

The recent study has demonstrated that, by varying the probe-polarization, the SC and PG responses were distinguished individually by spatial symmetry breaking accompanied by the SC and PG transitions in the cuprate superconductor $Bi_2Sr_2CaCu_2O_{8+\delta}$ (Bi2212) [29]. Since, on the CDW transition in a Q2D system spatial (translational and rotational) symmetries are broken, such a polarization-dependent pump-probe measurement will provide new information, especially on QP dynamics in terms of the second CDW transition.

In this paper, we report the use of pump-probe spectroscopy for a multiple CDW system of $DyTe_3$ with different probe polarizations. By performing concise symmetry analysis, we found that the observed anisotropic response for the probe is not only attributed to the CDW formation but also that it is quite sensitive to changes in the underlying lattice symmetry. Moreover, the ratio between anisotropic and isotropic responses shows unique anomalies associated with the first and second CDW transitions.

2. Experimental

$DyTe_3$ was chosen from among the RTe_3 compounds because the CDW formation occurs along two directions. It is thus expected to provide more information for symmetry analysis than the other unidirectional CDW compounds. The first CDW forms along the c axis just at room temperature ($T_{c1} \approx 305$ K) and along the the second a axis at T_{c2} of 50 K. In the series of RTe_3, a structural phase transition has not been reported except for the lattice modulation due to the CDW formation. This fact allows us to carry out simple analysis in terms of spatial symmetry breaking.

Single crystals of $DyTe_3$ were grown by a self-flux technique [35]. High-quality starting elements with the molar ratio Dy:Te = 1:10 were put into a quartz tube and sealed

under vacuum. Respective mixture were heated at 550 and 850 °C for 2 d. After heating, the mixtures were cooled gradually to 450 °C at a rate of 2 °C h^{-1} and quenched to room temperature. Clean sample surfaces were prepared by cleavage with adhesive tape. The crystalline axes were determined by x-ray diffraction measurement at room temperature. However, it was difficult to distinguish between the a and c axes because the resolution of the instrument was insufficient to detect a difference in their lattice constants.

In the optical pump-probe experiments, the pump beam excites carriers to a nonequilibrium high-energy state. This results in immediate relaxation of the excited carriers to states near the Fermi level by electron–electron and electron–phonon scattering [36]. When a gap for electronic excitation, such as a superconducting or CDW gap, is present, a relaxation bottleneck may occur and QPs accumulate just above the gap. The relaxation across the gap is caused gradually because of interaction between QPs and high-frequency phonons [12, 13]. The probe beam, which is delayed with the time t, measures the change of reflectivity, $\Delta R(t)$, which is connected with the non-equilibrium distribution of the QPs, Δf, as a function of t. The optical measurements were performed using 120 fs pulses centered at 400 nm for a pump ($F = 36\,\mu\text{J cm}^{-2}$) and 800 nm for a probe from a cavity-dumped Ti:sapphire oscillator with a repetition rate of 270 kHz. The pump and probe beams were coaxially overlapped by a dichroic mirror and irradiated perpendicular to the a–c plane. The probe pulse polarization was rotated by a half-wave plate. θ is the angle between the probe electric field and the direction tilted by 45° from a crystalline axis, as shown in figure 1(a).

3. Results

Figures 1(c)–(e) show transient reflectivity $\Delta R/R$ as a function of θ and $\Delta R/R$ for $\theta = 0°$ at $T = 310$, 200, and 20 K,
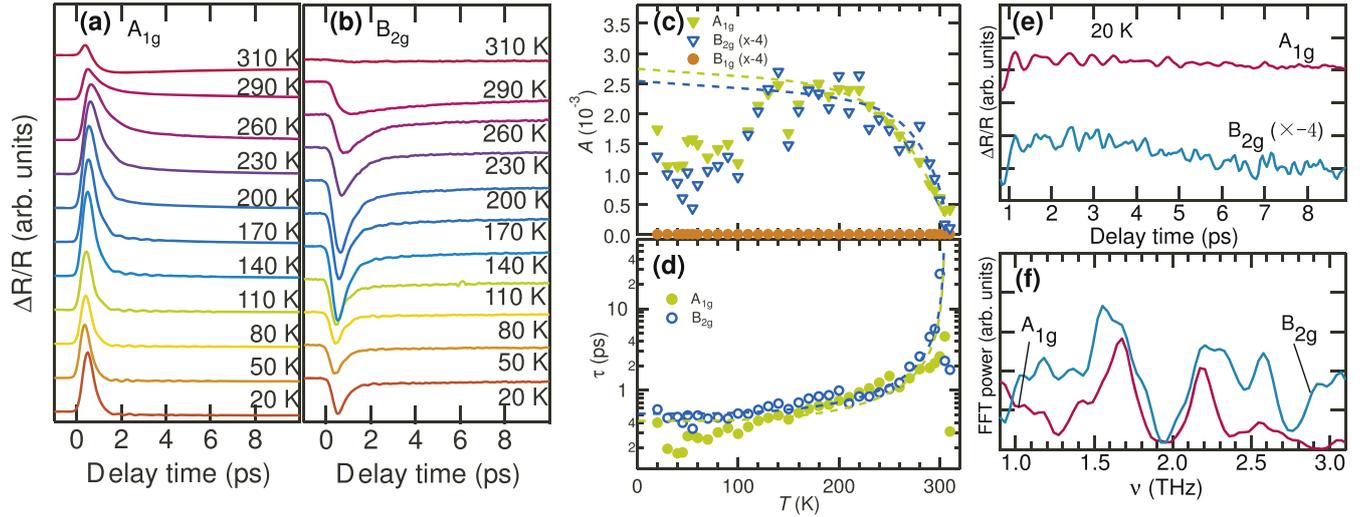
Figure 2. (a), (b) $\Delta R/R$ transients of the A_{1g} and B_{2g} components for various temperatures, respectively. The data are shifted for clarity. (c) Temperature dependence of the amplitude A of the A_{1g} and B_{2g} components. (d) Temperature dependence of the decay time τ of the A_{1g} and B_{2g} components The dashed lines display the result fitted by the theoretical model. (e) Oscillatory responses of the A_{1g} and B_{2g} components at 20 K. (f) Fourier-transform spectrum of the data in (e).

respectively. The maximum values of $\Delta R/R$ are plotted in figures (f)–(h). For $T = 310$ K ($T > T_{c1}$), the $\Delta R/R$ shows no angular dependence (isotropic). On the other hand, an anisotropic response is observed for $T = 200$ K ($T_{c2} < T < T_{c1}$). The signals are enhanced along the 135° and 315° directions, which correspond to the *a* or *c* axis. The anisotropy for the probe can be associated with the first CDW formation along with *c* axis. For $T = 20$ K ($T < T_{c2}$), the angular dependences is qualitatively similar to that for $T = 200$ K, although the second CDW occurs along the *a* axis.

The probe-polarization-dependent $\Delta R/R$ can be associated with two different types of pump excitation processe, stimulated Raman excitation and dissipative excitation (DE). The former is a coherent process and depends on the pump polarization, whereas the latter shows no pump polarization since information about the pump polarization is lost due to inelastic scattering. In our results, the observed anisotropy is independent of the pump polarization, indicating that DE is dominant. For the case of DE, the probe-polarization dependence of $\Delta R/R$ arises from the anisotropy of excited states affected by some symmetry breaking owing to the structural or electronic phase transition [29].

For DyTe$_3$, because the lattice constant of *a* is very close to that of *c* ($a \approx c$), it is reasonable to assume the tetragonal (D_{4h} point group symmetry). Under this assumption, the angular dependence of $\Delta R/R$ for the probe can be analyzed in the same way as the case of Bi2212 [29]. As a result, the photo-induced change of reflectivity is derived as

$$\frac{\Delta R}{R} \propto \Delta R^{A_{1g}} + \Delta R^{B_{1g}} \cos(2\theta) + \Delta R^{B_{2g}} \sin(2\theta), \quad (1)$$

where A_{1g}, B_{1g}, and B_{2g} correspond to symmetries in the *k*-space, as shown in figure 1(b), respectively. By fitting equation (1) to the angular dependences of $\Delta R/R$, we decomposed the data into the components of isotropic A_{1g}, anisotropic B_{1g}, and B_{2g} symmetries.

Figures 2(a) and (b) present $\Delta R/R$ transients of the A_{1g} and B_{2g} components, respectively, for various temperatures. As a result of the decomposition, the A_{1g} and B_{2g} components are found to develop with decreasing temperature, whereas the B_{1g} component is negligible at all temperatures. In the A_{1g} response, a combination of positive and negative components is observed at 310 K. As the temperature decreases, only the positive component develops, whereas a negative component dominates in the B_{2g} response. Oscillatory responses are seen in both the A_{1g} and B_{2g} channels at low temperatures, as shown later.

Since the maximum values A of $\Delta R/R$ are associated with the photo-induced QP density, n_{qp}, A is plotted as a function of temperature, as shown in figure 2(c). The curve of B_{2g} is qualitatively similar to that of the A_{1g} component. As the temperature decreases from 310 K and crosses T_{c1}, A increases steeply, indicating growth of the CDW gap. To explore the qualitative validity, we fitted the data with the theoretical model [13]. When n_{qp} is small as compared to the equilibrium conditions, $\Delta R/R$ is given by

$$\frac{\Delta R}{R} \propto \frac{\left(\Delta_{CDW}(T) + k_B T/2\right)^{-1}}{1 + g\sqrt{\dfrac{k_B T}{\Delta_{CDW}(T)}} \exp\left(-\dfrac{\Delta_{CDW}(T)}{k_B T}\right)}, \quad (2)$$

where $\Delta_{CDW}(T)$, k_B, and g indicate the BCS-type gap function, Boltzmann constant, and the ratio of bosonic and electronic densities of states that contribute to n_{qp}, respectively. The fits yield $\Delta_{CDW}(0) = 91$ and 88 meV for the A_{1g} and B_{2g} components, respectively. These values are close to those obtained in ARPES [32] and the previous pump-probe measurements [34].With a further decrease in temperature, the A values start to deviate from the model at around 130 K. Similar deviation has been observed in other RTe$_3$ compounds [34]. In the previous study, such a deviation may be associated with the resonant coupling between the
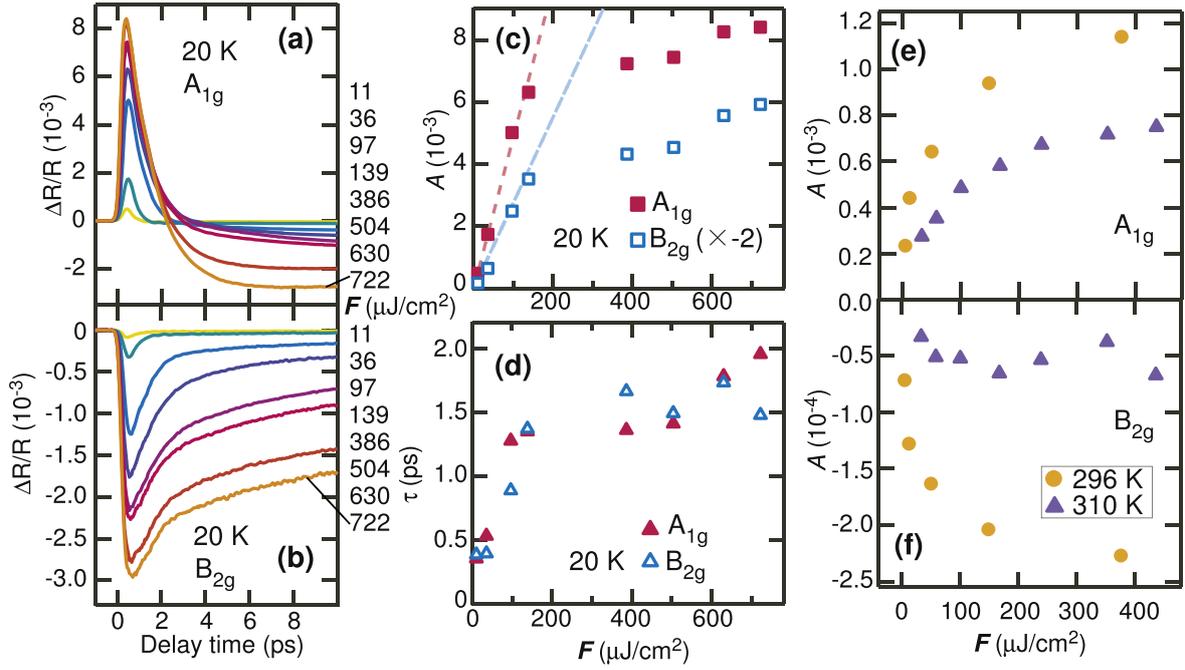
Figure 3. (a), (b) $\Delta R/R$ transients of the A_{1g} and B_{2g} components for various pump fluences at 20 K, respectively. (c), (d) Fluence dependence of amplitude and decay time of the A_{1g}, B_{1g}, and B_{2g} components, respectively. The dashed lines are linear fits. (e), (f) Fluence dependence of amplitude of the A_{1g} and B_{2g} components at 296 and 310 K, respectively.

collective excitation (amplitude mode) of CDW and the totally symmetric phonon [34]. Below 50 K, the A values tend to increase with decreasing temperature. The slight increase can be attributed to the occurrence of the second CDW.

Figure 2(d) shows the temperature dependences of the decay time obtained by fitting the rapid decline of the transient with a single-exponential function $A \exp\left(-\frac{t}{\tau}\right)$. Before fitting, to eliminate the contribution of the temperature-independent component from the data, we subtracted the result at 310 K from each results below 305 K for the A_{1g} response. The τ of both the A_{1g} and B_{2g} components show a clear divergence as T_{c1} is approached from below, whereas no pronounced anomaly is observed at T_{c2}. Theoretically, the relaxation time is associated with the CDW gap as $\tau \propto 1/\Delta_{CDW}(T)$ when $T \to T_{c1}$ [13] . This behavior agrees well with the divergence at T_{c1}. Therefore, we conclude that the positive component of the A_{1g} and B_{2g} response are associated with the CDW formation.

Figure 2(e) shows the oscillatory responses of the A_{1g} and B_{2g} components at a low temperature, where the relaxation component has been subtracted. The oscillations are observed not only in the A_{1g} channels but also the B_{2g} channels, although the oscillation amplitude in B_{2g} is more than 4 times smaller than that in A_{1g}. Figure 2 (f) exhibits the Fourier transform spectrum of the A_{1g} and B_{2g} oscillations. For the A_{1g} spectrum, the peak positions agree well with those in a previous report, [34] in which a mode at 2.2 THz corresponds to the collective excitation of CDW (amplitude mode) and the others are attributed to oscillations of the totally symmetric phonons. On the other hand, the spectrum of the B_{2g} component partly includes different modes. The

observed peaks in the B_{2g} channel may correspond to Raman-active phonon modes coupled with QPs in the B_{2g} symmetry.

Figures 3(a) and (b) present the $\Delta R/R$ transients of the A_{1g} and B_{2g} components, respectively, for various fluences at 20 K. For the A_{1g} response, in addition to a positive component, which is ascribed to the CDW formation, a long-lived negative component is seen at high fluences. This component probably corresponds to that observed at 310 K, indicating that it is unrelated to the CDW formation. In the B_{2g} response, two negative components seem to emerge at high fluences.

The maximum values of the A_{1g} and B_{2g} signals are plotted as a function of fluence in figure 3(c). Both the amplitudes have qualitatively similar fluence dependence. As the fluence increases, amplitudes increase linearly and shows a kink, followed by a gradual increase. We determined that the threshold fluence $F_{th} = 39\ \mu J\ cm^{-2}$ for both the A_{1g} and B_{2g} components by using the saturation model [20] . The F_{th} values are reasonable as compared to $47\ \mu J\ cm^{-2}$ for TbTe$_3$, which has a higher CDW transition temperature of 336 K [27]. Figures 3(e) and (f) show the fluence dependences of the amplitude of the A_{1g} and B_{2g} components, respectively, at high temperatures. The saturation behaviors are observed up to 310 K ($>T_{c1}$), indicating a precursor of CDW.

Figure 3(d) indicates the fluence dependence of decay time for the A_{1g} and B_{2g} signals. The τ value increases with increasing fluence, showing saturation behavior for both components. In the Rothwarf–Taylor (RT) model under the strong bottleneck condition [12], τ is given by

$$\tau^{-1} = 2\left(n_{qp} + n_T\right)\gamma, \qquad (3)$$

where n_{qp} is the photo-induced QP density, n_T is the QP density under the thermal equilibrium condition, and γ is the
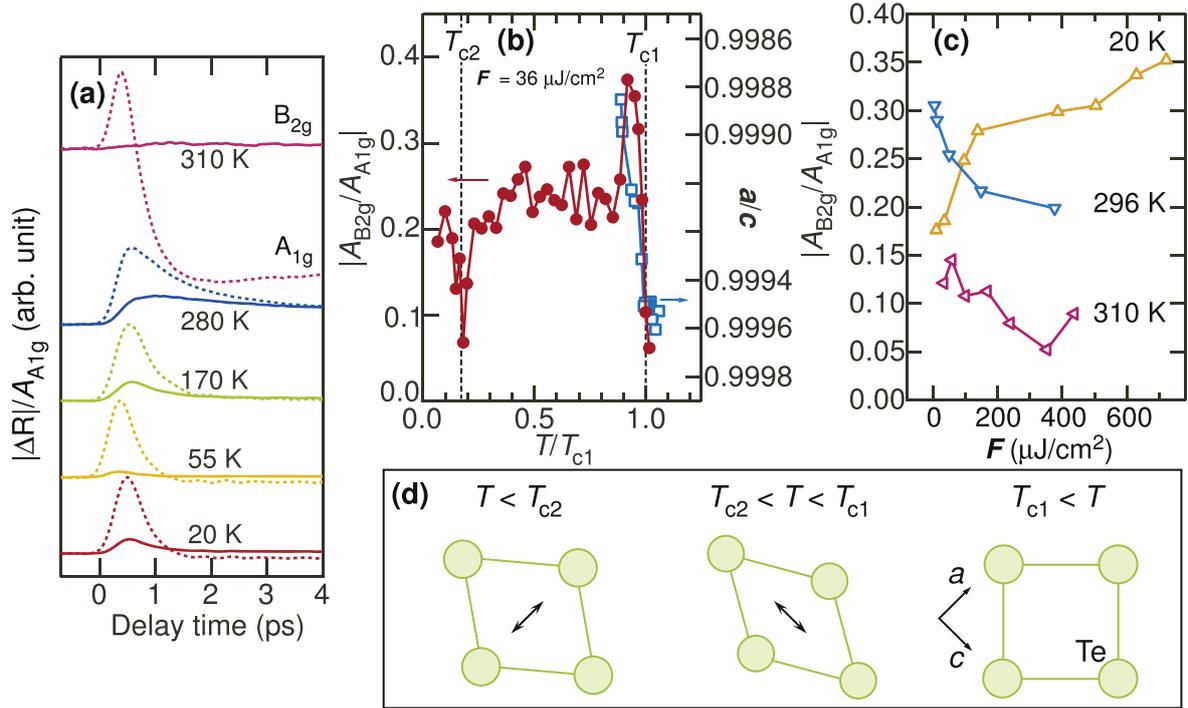
Figure 4. (a) Magnitude of transient reflectivity normalized by A in the A_{1g} component for various temperatures. The dashed and solid lines indicate the A_{1g} and B_{2g} components. The data are shifted for clarity. (b) Absolute values of ratio of A between the A_{1g} and B_{2g} components as a function of normalized temperature. Right axis is ratio of the lattice parameter between a and c in TbTe$_3$ adopted from [7]. (c) Fluence dependence of absolute values of ratio of A between the A_{1g} and B_{2g} components as a function of fluence for various temperatures. (d) Schematic of Te plane for three temperature regions.

effective relaxation rate. At low temperatures, n_T decreases as compared to n_{qp}, leading to the relation $\tau^{-1} \propto n_{qp}$ at low fluences. Our results are in contrast to the RT model. Although A increases linearly (figure 3(c)), τ seems to be proportional to n_{qp}, i.e., $\tau \propto n_{qp}$. Within the framework of the RT model, our results may be explained by the change of γ. If γ decreases with increasing fluence, it will lead to $\tau \propto n_{qp}$. This means that the bottleneck condition can be changed by varying the fluence. At high fluences, τ increases gradually. This behavior may be due to improper fitting. For both the A_{1g} and B_{2g} channels, $\Delta R/R$ seems to be two components at high fluences. Thus, use of a single exponential function will result in a poor fit. Similar behavior has been observed in Bi2212 [26].

As observed earlier, the temperature and fluence dependences of amplitude and decay time in the B_{2g} channel are quite similar to those in the A_{1g} channel. However, the following data reveal that the A_{1g} and B_{2g} responses have different origins. Figure 4(a) shows the magnitude of ΔR normalized by the maximum value A of the A_{1g} component for various temperatures. The ΔR value in the B_{2g} channel is obviously different from that in the A_{1g} channel. The ratio between the amplitude of the A_{1g} and B_{2g} components as a function of the normalized temperature is shown in figure 4(b). Strikingly, the ratio was found to increase near T_{c1} and, in contrast, decrease at T_{c2}. As the temperature increases from below T_{c1}, the $|A_{B_{2g}}/A_{A_{1g}}|$ curve shows a steep increase, followed by a rapid decrease. We note that the reduction above T_{c1} can be attributed to a negative component in the A_{1g}

channel, which is not associated with the CDW formation. For the intermediate temperature range $T_{c2} < T < T_{c1}$, there are almost no changes in the $|A_{B_{2g}}/A_{A_{1g}}|$ curve. Figure 4(c) shows the fluence dependence of $|A_{B_{2g}}/A_{A_{1g}}|$ for various temperatures. As the fluences increase, the $|A_{B_{2g}}/A_{A_{1g}}|$ curve shows a steep increase for 20 K, whereas it decreases for 296 and 310 K. At high fluences, all the curves become almost constant and monotonically shift downward with increasing temperature. These results indicate the distinct differences between A_{1g} and B_{2g} responses.

4. Discussion

Let us discuss origin of the isotropic A_{1g} and anisotropic B_{2g} responses. The A_{1g} component is determined by the CDW order parameter. Generally, the order parameter of broken symmetry ground states is complex, written as $\Delta = |\Delta| \exp(i\phi)$. Since in the excitation process by the pump pulse the dielectric constant is involved as powers of $|\Delta|^2$, it leads to the A_{1g} symmetry. Therefore, the steep growth of the A_{1g} signal below T_{c1} is assigned reasonably to the first CDW formation. The second CDW may be minor a contribution to the A_{1g} channel because there is no remarkable anomaly at around T_{c2} in figure 2(c). As shown in figures 2(e) and (f), it is reasonable that the amplitude mode of CDW was observed in the A_{1g} channel since it originates form the oscillatory modulation of $|\Delta|$.

The above discussion suggests that anisotropy of the CDW order parameter is not the origin of the B_{2g} component. However, our results indicate that both the B_{2g} and A_{1g} responses are dominated by the CDW order parameter. Thus, it is reasonable to assume that the origin of the anisotropic response is associated with changes in the underlying lattice and that the relation between the B_{2g} and A_{1g} transients is simply given by $\Delta R_{B_{2g}} = \beta \Delta R_{A_{1g}}$, i.e., $A_{B_{2g}} = \beta A_{A_{1g}}$, where β is a coefficient for the anisotropy and $|\beta|$ corresponds to $|A_{B_{2g}}/A_{A_{1g}}|$. In this case, we can explore the origin of the anisotropic transients (B_{2g} signal) by investigating the behavior of β. To compare $|\beta|$ with the anisotropy of the crystal structure, the ratio of the lattice parameters between a and c in TbTe$_3$, which is adopted from [33], is plotted on the right axis in figure 4(b). The ratio of the lattice parameters changes with decreasing temperature below T_{c1}, meaning that the lattice anisotropy grows monotonically. On the other hand, the $|\beta|$ curve shows a maximum just below T_{c1} and it is almost constant in the temperature range $T_{c2} < T < T_{c1}$. The comparison indicates that $|\beta|$ does not correspond linearly to the lattice anisotropy. The most remarkable feature is that $|\beta|$ varies only at T_{c1} and T_{c2}, suggesting that $|\beta|$ (B_{2g} signal) is not simply reflected by the lattice anisotropy but also by the anisotropy induced by the CDW transitions. When the temperature decreases and crosses T_{c1}, the underlying Te lattice deforms from a square to a rhombic shape as shown in the right side and middle of figure 4(d) owing to the first CDW formation along the c axis. In this case, the lattice anisotropy becomes strong, corresponding to enhancement of $|\beta|$ at T_{c1}. As the temperature decreases further, the second CDW forms along the a axis, deforming the lattice as shown on the left side of figure 4(d). At T_{c2}, the lattice anisotropy is weakened, in contrast to the case at T_{c1}. The decrease of the lattice anisotropy may lead to the suppression of $|\beta|$. In this way, the unique temperature dependence of $|\beta|$ is explained by the change of the lattice anisotropy induced by the CDW transitions.

The fluence-dependent variations of $|\beta|$ presented in figure 4(c) are also explained by the CDW-induced lattice anisotropy. For 20 K, the $|\beta|$ curve shows a steep increase with increasing fluence, and then it shows a kink followed, by a gradual increase. At high fluences, the $|\beta|$ values approach ~0.35, which is close to the value obtained near T_{c1}. When the fluence increases and exceeds F_{th}, the two CDWs are completely broken. This situation corresponds to the first CDW transition under varying temperature, indicating the enhancement of $|\beta|$. The contribution accompanied by the second CDW transition is difficult to detect since the F_{th} value of the second CDW is significantly smaller than that of the first one. Above 296 K, the $|\beta|$ curves decrease with increasing fluence. This behavior may trace the steep reduction of $|\beta|$ near T_{c1} with increasing temperature. For instance, at 296 K, the $|\beta|$ values are ~0.3 at low fluences and ~0.2 at high fluences. These values are consistent with those obtained at 295 and 300 K. At high temperatures, since the large negative component in the A_{1g} channel is significantly larger than that at 20 K and it contributes significantly to the fluence dependence of $|\beta|$.

From the above discussions, the appearance of the B_{2g} response is interpreted as a consequence of spontaneous symmetry breaking in terms of the CDW transition. Usually, for a one-dimensional CDW system, the translational symmetry is broken. On the other hand, for the two-dimensional system, in addition to the translational symmetry, the rotational symmetry is broken simultaneously due to unidirectional CDW formation. In the case of DyTe$_3$, as a result of such the symmetry breaking, the symmetry of the system changes from tetragonal to orthorhombic below T_{c1}. This is consistent with the fact that the B_{2g} signal is enhanced along the crystalline axis (a or c), which corresponds to the first CDW wave vector, $\boldsymbol{q}_1$, or to the direction perpendicular to $\boldsymbol{q}_1$. In our results, anisotropy in the B_{2g} channel is conserved as the temperature decreases and crosses T_{c2}, indicating that the reduced rotational symmetry is maintained even though the second CDW occurs. Since the absolute value of the second CDW wave vector, $\boldsymbol{q}_2$, is not identical to that of $\boldsymbol{q}_1$ for ErTe$_3$, [33] the orthorhombicity will not be changed even for DyTe$_3$ below T_{c2}. Consequently, the emergence of the anisotropic transients corresponds to occasion of the rotational symmetry breaking accompanied by the CDW transition. The first CDW transition occurs with the translational along the c axis and rotational symmetry breaking, while only the translational symmetry along the a axis is broken at the second CDW transition, maintaining the rotational symmetry.

Our results clearly show that the B_{1g} component is absent in the whole temperature range. The B_{1g} symmetry corresponds to the direction tiled by $\sim45°$ from the crystalline axis (Te–Te bond direction) in real space. In the previous measurements [31, 33], any charge or lattice modulations along the direction have not been observed in the RTe$_3$ compounds, which are consistent with our measurements.

Finally, we compare our results with the results of Bi2212 [29]. In Bi2212, below $T^{\star}$, not only anisotropic B_{2g} response but also isotropic A_{1g} response are observed. A of B_{2g} component is about 9 and 14 times (for over- and under-doped sample) smaller than that of A_{1g} component. The ratio between the A_{1g} and B_{2g} component in Bi2212 is larger than that of in DyTe$_3$. Moreover, the temperature dependence shows A increases gradually as temperature increases, which is contrast to that in DyTe$_3$. These differences between Bi2212 and DyTe$_3$ can be originated from spatial inhomogeneity. In Bi2212, spatial variations of carrier density and superconducting gap were observed [39, 40]. Thus, domains of some electronic ordered state accompanied by the B_{2g} symmetry breaking can be emerged in the sample below $T^{\star}$. On the other hand, unidirectional CDW is formed uniformly in real space below T_{c1} in DyTe$_3$. Since order parameter is averaged totally as the domains are spatially distributed, magnitude of the order parameter will be smaller than that in the case where electronic ordered state is spatially homogeneous. This may be the reason why the ratio between the A_{1g} and B_{2g} component and temperature dependence of A are different between them.

5. Conclusion

By performing pump-probe spectroscopy with different polarizations for the probe photons in DyTe$_3$, we detected successfully not only the first CDW transition but also the second one in the ratio between the A$_{1g}$ and B$_{2g}$ components. These polarized measurements enabled us to investigate a buried component in multiple component systems more easily than we could using normal measurements. It thus provides a significant advantage for investigating the competition and coexistence of multiple electronic ordered phases.

Acknowledgments

References

[1] Zewail A H J 1993 *Phys. Chem.* **97** 12421
[2] Knox W H, Hirlimann C, Miller D A B, Shah J, Chemla D S and Shank C V 1986 *Phys. Rev. Lett.* **56** 1191
[3] Shank C V, Fork R L, Yen R, Shah J, Greene B I, Gossard A C and Weisbuch C 1983 *Solid State Commun.* **47** 981
[4] Rizo P J, Pugzlys A, Slachter A, Denega S Z, Reuter D, Wieck A D, van Loosdrecht P H M and van der Wal C H 2010 *New J. Phys.* **12** 113040
[5] Hase M, Katsuragawa M, Constantinescu A M and Petek H 2013 *New J. Phys.* **15** 055018
[6] Decurtins S, Gutlich P, Kohler C P, Spiering H and Hauser A 1984 *Chem. Phys. Lett.* **105** 1
[7] Koshihara S, Tokura Y, Takeda K and Koda T 1992 *Phys. Rev. Lett.* **68** 1148
[8] Miyano K, Tanaka T, Tomioka Y and Tokura Y 1997 *Phys. Rev. Lett.* **78** 4257
[9] Fiebig M, Miyano K, Tomioka Y and Tokura Y 1993 *Science* **97** 12421
[10] Timusk T and Statt B 1999 *Rep. Prog. Phys.* **62** 61
[11] Krasnov V M, Yurgens A, Winkler D, Delsing P and Claeson T 2000 *Phys. Rev. Lett.* **84** 5860
[12] Rothwarf A and Taylor B N 1967 *Phys. Rev. Lett.* **19** 27
[13] Kabanov V V, Demsar J, Podobnik B and Mihailovic D 1999 *Phys. Rev. B* **59** 1497
[14] Demsar J, Podobnik B, Kabanov V V, Th Wolf and Mihailovic D 1999 *Phys. Rev. Lett.* **82** 4918
[15] Kaindl R A, Woerner M, Elsaesser M, Smith T, Ryan D, Farnan J, McCurry G and Walmsley M 2000 *D Science* **287** 470
[16] Averitt R D, Rodriguez G, Lobad A I, Siders J L W, Trugman S A and Taylor A J 2001 *Phys. Rev. B* **63** 140502(R)
[17] Dvorsek D, Kabanov V V, Demsar J, Kazakov S M, Karpinski J and Mihailovic D 2002 *Phys. Rev. B* **66** 020510
[18] Demsar J, Averitt R D, Taylor A J, Kabanov V V, Kang W N, Kim H J, Choi E M and Lee S I 2003 *Phys. Rev. Lett.* **91** 267002
[19] Liu Y H, Toda Y, Shimatake K, Momono N, Oda M and Ido M 2008 *Phys. Rev. Lett.* **101** 137003
[20] Kusar P, Kabanov V V, Sugai S, Demsar J, Mertelj T and Mihailovic D 2008 *Phys. Rev. Lett.* **101** 227001
[21] Luo C W, Lo H P, Su C H, Wu I H, Chen Y J, Wu K H, Lin J Y, Uen T M, Juang J Y and Kobayashi T 2010 *Phys. Rev. B* **82** 104512
[22] Mertelj T, Kabanov V V, Gadermaier C, Zhigadlo N D, Katrych S, Karpinski J and Mihailovic D 2009 *Phys. Rev. Lett.* **102** 117002
[23] Gadermaier C, Alexandrov A S, Kabanov V V, Kusar P, Mertelj T, Yao X, Manzoni C, Brida D, Cerullo G and Mihailovic D 2010 *Phys. Rev. Lett.* **105** 257001
[24] Gong Y, Lai W, Nosach T, Li L J, Cao G H, Xu Z A and Ren Y H 2010 *New J. Phys.* **12** 123003
[25] Giannetti C *et al* 2011 *Nat. Commun.* **2** 353
[26] Toda Y, Mertelj T, Kusar P, Kurosawa T, Oda M, Ido M and Mihailovic D 2011 *Phys. Rev. B* **84** 174516
[27] Stojchevska L, Kusar P, Mertelj T, Kabanov V V, Toda Y, Yao X and Mihailovic D 2011 *Phys. Rev. B* **84** 180507(R)
[28] Luo C W, Wu I H, Cheng P C, Lin J Y, Wu K Y, Uen T M, Juang J Y, Kobayashi T, Chareev D A, Volkova O S and Vasiliev A N 2012 *Phys. Rev. Lett.* **108** 257006
[29] Toda Y, Kawanokami F, Kurosawa T, Oda M, Madan I, Mertelj T, Kabanov V V and Mihailovic D 2014 *Phys. Rev. B* **90** 094513
[30] Norling B K and Steinfink H 1996 *Inorg. Chem.* **5** 1488
[31] DiMasi E, Aronson M C, Mansfield J F, Foran B and Lee S 1995 *Phys. Rev. B* **52** 14516
[32] Brouet V *et al* 2008 *Phys. Rev. B* **77** 235104
[33] Ru N, Condron C L, Margulis G Y, Shin K Y, Laverock J, Dugdale S B, Toney M F and Fisher I R 2008 *Phys. Rev. B* **77** 035114
[34] Yusupov R V, Mertelj T, Chu J H, Fisher I R and Mihailovic D 2008 *Phys. Rev. Lett.* **101** 246402
[35] Sinchenko A A, Lejay P and Monceau P 2012 *Phys. Rev. B* **85** 241104(R)
[36] Allen P B 1987 *Phys. Rev. Lett.* **59** 1460
[37] Stevens T E, Kuhl J and Merlin R 2002 *Phys. Rev. B* **65** 144304
[38] Lavagnini M *et al* 2008 *Phys. Rev. B* **78** 201101(R)
[39] Howald C, Fournier P and Kapitulnik A 2001 *Phys. Rev. B* **64** 100504
[40] Pan S H *et al* 2001 *Nature* **413** 282